

## **Appendices**

### **Appendix 1: Experimental Details**

#### Initial Analyses

Initial measurements of whole core susceptibility were conducted at the Limnological Research Center (LRC) using a Bartington susceptibility meter equipped with a MS2C loop sensor (diam. = 10 cm). The measuring interval was 2 cm, but the spatial resolution of is thought to be on the order of approximately 10 - 20 cm. Whole core magnetic susceptibility was used for initial core correlation for cores PB 94 1-5, is not used for any of the subsequent analyses. Soon after retrieving the cores they were split lengthwise at the LRC, photographed, described and subsampled for further analysis. Sampling interval for magnetic studies was less than 2 cm and samples were packed into plastic boxes of 5.28 cm<sup>3</sup> volume. Samples from core PBAS 94-5a were dried in air prior to the Rock magnetic measurements, samples from cores PBAS-96 were kept moist and cool until all measurements were conducted and then dried at room temperature under vacuum.

#### Chemical Composition

The chemical composition of Pittsburg Basin, sites PBAS 94-5a and PBGP-95 was determined using a Perkin-Elmer/Sciex Elan 5000 inductively coupled plasma mass spectrometer (ICP-MS). A suite of 14 major and 19 trace elements was measured for both sites. In addition, rare earth elements were measured for site PBGP-95.

X-ray diffraction analyses were performed on magnetic extracts using a Philipps Series 3100 X-Ray generator, equipped with a Norelco automated step scanner. The scans were analyzed using Jade analytical software for background subtraction, peak finding and matching. Lattice parameters were calculated from a minimum of 4 identified peaks. SEM images (backscattered and secondary electron images) and energy dispersive X-ray spectra (EDS) were obtained from magnetic extracts on a JEOL 840 II scanning electron microscope (accelerating voltage 20 keV). The magnetic fraction used

for these analyses was obtained by circulating a slurry of the sample past the field of a strong magnet for several days as outlined by [Petersen *et al.*, 1986].

### Dating

We attempted to date the sediments of Pittsburg Basin by  $^{14}\text{C}$ -AMS dating of a plant macrofossil and several Infrared Stimulated Luminescence (IRSL) dates, obtained from cores PBAS-94 5e and PBAS 96-1. The details for the radiocarbon date will be discussed by [Teed, in prep.]. For IRSL dating 10 cm long segments of unsplit core material were supplied to Dr. S. Balescu, Université du Québec à Montréal [Balescu, unpublished data].

### Total Organic Carbon

Total organic carbon was determined by the “loss on ignition” method [Dean, 1974]. Samples were placed in Al dishes, oven dried and heated to  $500^{\circ}\text{C}$  for 2 h. TOC is calculated from the weight loss  $\Delta m$  between the oven-dried and the ignited sample with  $\text{TOC} = 2.13 * \Delta m$ . The aluminum dishes were heated to  $500^{\circ}\text{C}$  overnight prior to the TOC measurement to burn off the oil coating of the dish.

### Particle Size Distribution

To estimate the particle size distribution the gravel and sand fractions were separated by sieving (2mm,  $63\mu\text{m}$  sieves), while the clay fraction ( $< 2\mu\text{m}$ ) was separated by centrifugation.

### Specific Surface Analysis

see appendix 2

### Magnetic Susceptibility

Magnetic susceptibility at room temperature has been measured using a Bartington susceptibility meter MS-1 and a Geofyzika Kappabridge KLY-2. Frequency-dependent susceptibility  $\chi_{FD}$  was measured at 20 frequencies between 40 and 4000 Hz at room temperature using a Lakeshore Series 7000 susceptometer.

### Remanence Parameters

ARM and pARM were acquired in a modified Schonstedt AC demagnetizer (model GSD-1) using a bias field of 50  $\mu$ T and a maximum alternating field of 99 mT. SIRM was acquired in a DC field of 1.5 T. All remanence parameters were measured using a 2G superconducting rock magnetometer (model 760-R). The magnetic remanence of strongly magnetic samples were measured using a Schonstedt spinner magnetometer (model SSM-1). S-ratios were calculated for a SIRM given in a DC-field of 1.5T and a DC-backfield of 0.3T. IRM was acquired in DC fields. All DC fields were produced by the electromagnet of our VSM.

### Hysteresis Loops

Hysteresis loops for samples from Pittsburg Basin were measured on a Vibrating Sample Magnetometer (VSM) constructed in our laboratory. The maximum field was 1 T. For Kirchner Marsh hysteresis parameters were measured on a Princeton Measurement Corporation Micro-Vibrating Sample Magnetometer ( $\mu$ VSM). The maximum field ranged between 800mT and 1T.

### Curie temperatures

Curie temperatures were estimated from measurements of magnetic susceptibility vs. temperature using the Kappabridge. The heating experiments were conducted in argon and air between room-temperature and a maximum temperature of 700°C. The heating rate is approximately 7.5°C/min.

Measurements of saturation magnetization  $J_s$  vs. temperature were conducted for the same temperature range using the  $\mu$ VSM. These measurements were performed in a helium atmosphere.

#### Thermal Demagnetization, TRM acquisition

Some samples were thermally demagnetized using a Schonstedt Thermal Specimen Demagnetizer (model TSD-1). TRM acquisition was performed in a field of  $50 \mu\text{T}$ , using a furnace constructed at the IRM.

#### Low-temperature experiments

Low-temperature measurements were performed on a Quantum Design MPMS-2 magnetic properties measurement system between temperatures from 5K to 300K. For field-cooled measurements the samples were cooled in the presence of a field of 2.5T, for zero field cooled measurements the samples were cooled in zero-field and acquired a remanence at 9K in a field of 2.5T.

## Appendix 2: Specific Surface Area Measurements

Specific surface area measurements rely on the adsorption of a monomolecular layer on all the surfaces of a clay particle. If the thickness and density of the adsorbed layer are known it is possible to calculate the size of the area coated by the adsorbate. The adsorbate can be water vapor [Newman, 1983], N<sub>2</sub> gas [Makower *et al.*, 1937], or a polar liquid such as ethylene glycol monoethyl ether (EGME) [Carter *et al.*, 1965; Cihacek and Bremner, 1979; Eltantawy and Arnold, 1973; Heilman *et al.*, 1965]. As pointed out by several authors [Carter *et al.*, 1986; Churchman *et al.*, 1991; Tiller and Smith, 1990], neither method is likely to produce results in terms of absolute surface area, because some of the underlying assumptions are rarely met in experiments. The main sources of error are incomplete coating of all surfaces (internal and external) and the achievement of a monomolecular layer thickness. Nevertheless it is possible to obtain information about relative changes in SSA within a sample set.

Measurements of specific surface area (SSA) were conducted following the recommendations by [Carter *et al.*, 1986; Tiller and Smith, 1990]. Samples were gently ground up and organic matter was removed by treatment with NaOOH. The clay fraction was separated by centrifugation and placed in an Al weighing dish, outfitted with an Al-lid. Dry weight of the clay fraction was determined after drying the sample at 110°C overnight. Only the clay fraction was used in the determination of SSA. The samples were allowed to equilibrate with EGME for 45 minutes at room-temperature. Excess EGME was then removed by evaporation at a pressure of approximately 15 Pa (0.1 T) at the presence of excess EGME and CaCl<sub>2</sub> as a drying agent. Weight loss was monitored over 36h at 12h intervals. The drying agent was recycled after each run crushing it and heating it to 270°C for 24h [Holleman and Wiberg, 1985].

Assuming a specific surface area of 50 m<sup>2</sup>/g for kaolinite and 700 m<sup>2</sup>/g for montmorillonite [Scheffer and Schachtschabel, 1992], the following weight gain due to the adsorption of EGME on all surfaces is expected:

$$A = \frac{W_a}{W_s * 0.000286} \quad [\text{Carter et al., 1986}]$$

where  $A$  = specific surface area of the sample in  $m^2/g$

$W_a$  = weight of EGME retained in g

$W_s$  = weight of dried sample in g

using the SSA's mentioned above the expected weight gain due to EGME adsorption for 1g of sample is:

$W_a = 0.0143$  g (Kaolinite)

$W_a = 0.2002$  g (Montmorillonite).

Estimated error of measurement:

Sample masses ranged between 0.48 g and 0.14 g. The accuracy of the scale used for the experiments was estimated as  $\Delta m = 0.00025$  g. This is less than the theoretical accuracy of the scale, which is 0.00002 g and takes into account that the measurements are made rapidly to minimize the adsorption of water on the air dried samples during the weighing process. The error estimate was obtained by measuring an air dried soil sample ten times. Using this weighing error the error of the SSA due to inaccurate mass determination is:

$$\begin{aligned} \Delta SSA &\approx \frac{\partial SSA}{\partial W_a} \Delta W_a + \frac{\partial SSA}{\partial W_s} \Delta W_s \\ &= \frac{B}{W_s} \Delta W_a + \frac{W_a B}{W_s^2} \Delta W_s \end{aligned} \quad (\text{eq. A2.1})$$

where  $B = 0.000286$ .

Assuming a measurement error of  $\Delta m = 0.00025$ g the error associated with  $W_a$  and  $W_s$  is

$$\begin{aligned} W_a &= W_{\text{saturated}} - W_{\text{ovendried}} \\ \Delta W_a &= \Delta W_{\text{saturated}} - \Delta W_{\text{ovendried}} \\ \Delta W_a &= 2 * 0.00025g = 0.0005g \end{aligned}$$

The same measurement error applies to  $W_s$ . The constant B is poorly constrained [Tiller and Smith, 1990], however, any error in B will only expand or compress the results but leave the relative proportions intact.

Since it is unlikely that all the assumptions such as monomolecular layer thickness and complete coating of all surfaces are fulfilled, it is expected that the measurement error in weight determination is accompanied by systematic errors, which are hard to estimate *a priori*. Such errors, which can vary from sample to sample, include imperfect development of the “monomolecular layer”, but also the adsorption of water to the samples during weighing. Therefore, a second approach tried to estimate the total error associated with the measurement by repeatedly measuring a well defined clay sample of (supposedly) known surface area. Several SSA determinations were performed on a Namontmorillonite from Clay Sur, WY, which can be obtained from the Clay Repository of the University of Missouri (sample SWy-2). Table A1 lists the measured SSA's and the errors due to inaccurate weight determination. The measurement error determined from the set of 10 measurements is nearly twice as high as the error due to the weighing process alone. The error bars in Figure 7.7 are twice the measurement error as obtained by equation A2.1 and reflect the presence of systematic errors in the data set. [Tiller and Smith, 1990] obtains an SSA value of 720 m<sup>2</sup>/g for a sample from the same locality. Our results are in the same ballpark, but show that absolute values of SSA should be taken with a grain of salt.

Specific Surface Areas For Na-Montmorillonite Standard

	SSA (m <sup>2</sup> /g)	Δ SSA
	792	11.1
	752	19.3
	783	12.1
	709	11.0
	749	17.2
	772	16.6
	716	7.2
	752	9.0
	742	13.7
	737	16.7
average:	750.4	13.4
standard deviation of one measurement:	25.3	

**Table A1:** Specific surface area for Na-Montmorillonite standard. Errors in left column are measuring errors due to incorrect weight determination. They do not include systematic errors, which are reflected in the standard deviation of the samples.

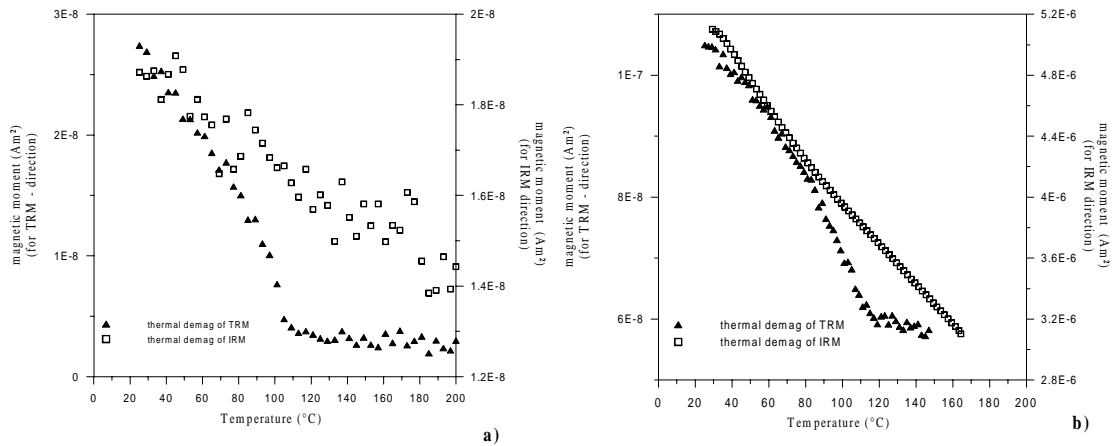
### Appendix 3: Test for Goethite

Goethite is a magnetically hard mineral that could explain the observed variations in S-ratios as observed in many lake sediments and soils. It is however hard to detect because it occurs in low concentrations in the sediment, is often poorly crystalline and its saturation magnetization is very low (goethite:  $M_s \approx 2$  kA/m; magnetite:  $M_s \approx 480$  kA/m [Dunlop and Özdemir, 1997], p. 51). Standard experiments such as XRD or measurements of magnetic properties are therefore unlikely to detect the presence of goethite.

The following experiment has been designed as a potential test for the presence of goethite in a natural sample. It exploits the fact that goethite has a very low Néel temperature ( $T_N \approx 120$  K, [Özdemir and Dunlop, 1996] but is very hard to magnetize at room temperature. Simple thermal demagnetization of a goethite bearing sample might not yield a good blocking- or Néel temperature because the demagnetization of a soft and much stronger magnetite or maghemite component overshadows the subtle loss in magnetic moment due to the demagnetization of the goethite component. The modified demagnetization experiment involves several steps: A TRM is acquired at  $140^\circ\text{C}$ . The relatively low acquisition temperature is well above the Néel temperature for goethite, but well below the Néel temperature of hematite. Maximum temperatures are also low enough to avoid a thermal alteration of the sample. The sample is then demagnetized in an alternating field of 100 mT (or stronger if possible - 300mT would be desirable) to remove any magnetic remanence due to magnetically soft minerals. The final step involves stepwise thermal demagnetization of the sample, which should show a characteristic drop in remanence near  $120^\circ\text{C}$  if goethite is present.

Various variations of the experiment are possible. It is, for example, possible to apply a TRM, followed by an IRM applied at a direction orthogonal to the original TRM direction. A similar experiment was already suggested by [Lowrie, 1990]. A simultaneous demagnetization of two or more components, however, might not work for some cryogenic magnetometers if one of the components is orders of magnitudes weaker than the strongest component. The three Squid sensors of our 2G superconducting rock

magnetometer (2G SRM, series 760R) are not completely independent from each other and a very strong magnetic moment measured along one particular axis will affect the readings of the other two sensors. Aside from this instrumental shortcoming (which might be a particular feature of our seasoned instrument) it is difficult to assure exact orthogonality of the TRM and IRM components. This approach, however can work for some specific instruments. Figures A3a,b show the thermal demagnetization curves for a TRM, carried by goethite and an IRM, acquired after TRM acquisition, at an orthogonal direction. The experiment was conducted using a  $\mu$ VSM, which allows for very precise sample orientation and the exact measurement of one specific component. The TRM demagnetization clearly shows the Néel temperature of goethite, even when the sample



consists of a mixture of goethite and magnetite (Figure A3b).

**Fig. A3:** **a)** Thermal demagnetization curves for synthetic goethite sample (Pfizer YLO 3288D lot 102). The TRM demagnetization curve clearly shows the unblocking of goethite between 110°C and 120°C. IRM demagnetization (IRM acquired after TRM acquisition in a 1T field, orthogonal to TRM direction) shows no evidence of any goethite unblocking. **b)** Same experiment but for a sample consisting of a goethite - magnetite mixture (goethite : maghemite = 5.6:1, goethite as in a), magnetite: Wright 4000,  $d \approx 0.05\mu\text{m}$ )

Figure A3 clearly shows the unblocking of goethite, even in the presence of a magnetite component. The technique has been applied to a variety of synthetic samples and showed good results for synthetic sample mixes. Up to today, however, the method has not been applied successfully to a natural sample. This may be due to the fact that all natural samples had only very low concentrations of goethite, since the abundance of goethite in

these samples was not measured by an independent method. A second explanation is that naturally occurring goethite is magnetically softer (probably due to its poor crystallinity or small grain-size) and is affected by either IRM acquisition or AF demagnetization.

## Appendix 4: Lithology of Pittsburg Basin

### Site PBAS 94-5a

All drives drilled with Mobile hollow stem augur, no liners. Depths are given as revised depths (with respect to master cores 94-5b-d). Original depths are given in parentheses. Bold face numbers mark key horizons used in core correlation

Drive #	original depths (cm)	revised depths (cm)	Notes
1	0-117		gray - brown silty clay, heavily mottled, top layer disturbed by plowing
2 upper	117-217	115-215	rusty to less rusty to gray-brown, gradational transition
2 lower	217-267	215-265	
			(214 - 244) gray silty clay
		242	(244- 267) black crumbly peat
3	269-380	269-357	
			269-295 (269-295) black, crumbly peat, no shells
			295-333 (295-356) massive, dark brown, stretched by 23 cm
		333	333-357 (356-374) black, shelly peat
			351-357 (374-380) brownish black silty peat
Gap, 395-416 section missing			
4 upper	424-524	424-524	top deeper than 418 cm
			(424-438) dark brown silt, some shells
		440	(438-449) black, abund. shells, coarser silt
			(449-504) gray brown, few shells, massive finer silt
			(504-505) light gray clay layer
			(505-520) dk brown, massive, more clay
			(520-523) dk brown, somewhat crumbly
4 lower	524-584	524-570?	

			(520-561) dk. brown, somewhat crumbly clay
		560	560 - 570 (561-584) gray brown to gray green silty clay with brown veins in upper 6 cm, STRETCHED
5 upper	556-656	570?-660	
			570-660 (554-654) gray green clay STRETCHED
5 lower	656-718	660-721	
			660-675 (654-669) gray green silty clay
		680	675-692 (669-687) banded alternating lt. and dk. brown
		692	692-722 (687-721) dk. brown fissile peat
6 upper	739-792	730-782	
			730-736 (739-745) dk brown to black
		736-738	736-739 (745-748) finely laminated dk. gray layers with white layers
			739-755 (748-765) brown, weakly fissile silty clay
			755-762 (765-772) lighter brown, finely laminated
		761	762-782 (772-792) gray, clayey silt, massive
6 lower	792-892	782-882	
			(782-800) gray, clayey silt, massive
		800	(800-842) banded gray and brown alternating layers
		845	(842-882) weakly banded dk & lt. gray
sand blew up hole - end of drive			

Site 96-2

All cores drilled with a Livingston piston corer, attached to Giddings soil probe. Depths are original depths in cm. Colors given as Munsell colors.

drive #	depth	comments
1 (425-475)	425-431	black peat, abundant shells (5Y 2.5/1)
	431-440	black, very few shells
	440-445	black, abundant shells
	445-470	black (5Y 2.5/1) silty clay, few shells
	470-475	conc. of white grains and shell fragments , abrupt transition (trash from top)
2 (475-525)	475-478	disturbed layer
	478-488	black (5Y, 2.5/1) peat, few shells, more clay than below
	488-504	black , fissile peat
	504-512	black crumbly peat
	512-525	lost
3(525-575)	525-552	black (5Y, 2.5/1) fissile peat with stringers of lighter colored material
	552-556	mixed layer, olive gray clay (5Y, 5/2)
	556-563	gray clay (5Y, 5/1) with very small darker dots, abrupt contact to lower layer
	563-575	dark gray clay (2.5Y, 4/1), homogenous
4(575-625)	575-596	dark gray clay as above
	596-609	as 556-563, surface seems rougher
	609-625	gray clay (5Y, 5/1)
5(625-675)	625-646	dark gray (5Y, 4/1) homogenous clay
	646-658	banded, alt. olive gray (5Y, 4/2) black (5Y, 2.5/1) layers
	658-666	black , fissile peat, slight banding visible)
	666-675	black fissile peat
6 (675-725)	675-687	black (5Y, 2.5/1) crumbly peat this black layer (646 - 695) was orange brown when first removed from the lake!

	687-705	transitional zone, getting lighter colored with depth, some banding
	705-720	dark gray (5Y, 4/1) silty clay, dense
7 (725-775)	725-742	dark gray clay, some lighter colored specks
	742-755	alternating lt. - dk. bands
	755-774	finely laminated clay
	774-775	dark gray clay
8 (775-825)	775-785	dark gray clay
	785-805	groups of darker laminae in dark gray clay
	805-815	gray clay (5Y, 5/1) sandier, sandy bottom, can hear scratching at bottom layer

**Appendix 5: Lithology of Pittsburg Basin Gravel Pit (PBG-95)**

Sampled 19-6-1995 by B. Curry (ISGS) and Ch. Geiß. All depths with respect to modern soil surface.

Depth (cm)	Formation	Comments	
0-16	Peoria Silt	modern E horizon, light colored, powdery silt	I E
16-34		modern Bt, fine subang. block	I Bt
34-50		modern Bt, coarse subang. block, Mn stains	I Bt
50-100		modern C, common Mn stains, vert. cracks filled with gray fine material (silts), rest oxidized yellowish brown	I C3
100	Roxana Silt	darker brown, sandier, some gravel, ped break easily, weakly developed Farmdale at top of unit (slightly more structure)	IIC3
100-200		coarse silt, increase of clayskins along root-channels, abundant pores, peds break harder, classified as Sangamon soil, however parent material seems to be Roxana silt.	IIIA
200-230		increase in clayskins, pores, no obvious root patterns, transitional zone to Hagarstown gravels	IIIBt
230-345	Hagarstown gravel	coarse gravel, gravelly sand, abundant Mn stains, large pores, thick clayskins, sticky, extremely hard when dry	IV Bt
345-390		red sand, slightly sticky, Mn blotches, weak structure	V Bt
390-460		coarse gravel, gravelly sand, less Mn stains and clay than 230 - 345	IV Bt
460-505		red sand slightly sticky, no structure	V Bt
505-		loose coarse sand, fine gravel, gleyed, gray-brown	VI C

## Appendix 6: Common and Scientific Names of Plants

In the text plants are generally referred to by their common names, while their scientific names are given in the pollen diagrams and figures. Using common names has the advantages that the text is more readable for readers unfamiliar with botanical names but with a general knowledge of trees and shrubs. However, many of the common names do apply to more than one species. Black ash, for example is used for both *Fraxinus nigra* and *Fraxinus pennsylvanica* [Peattie, 1991], which can be misleading in an analysis of the pollen diagrams. For that reason these diagrams are labeled with their scientific names. The following table lists all the plants mentioned in the text by their common and scientific name.

<b>Scientific Name</b>	<b>Common Name</b>	<b>Scientific Name</b>	<b>Common Name</b>
<b>Trees</b>		<b>Herbs</b>	
<i>Alnus</i>	alder	<i>Ambrosia</i>	ragweed
<i>Betula</i>	birch	<i>Artemisia</i>	wormwood/sage
<i>Carpinus</i>	ironwood	<i>Asteraceae</i>	
<i>Carya</i>	hickory	<i>Chenopodiaceae</i>	goosefoot
<i>Celtis</i>	hackberry	<i>Cyperaceae</i>	sedges
<i>Corylus</i>	hazel	<i>Humulus</i>	hops
<i>Fagus</i>	beech	<i>Poaceae</i>	sedges
<i>Fraxinus</i>	ash		
<i>f. nigra</i>	black ash		
<i>f. pennsylvanica</i>	red ash		
<i>Juglans</i>	walnut	<b>Aquatics</b>	
<i>Juniperus</i>	juniper	<i>Myriophyllum</i>	milfoil
<i>Liquidambar</i>	sweetgum	<i>Typha</i>	cattails
<i>Ostrya</i>	hornbeam	<i>Zizania</i>	
<i>Picea</i>	spruce		
<i>Pinus</i>	pine		
<i>Platanus</i>	sycamore		
<i>Populus</i>	poplar		
<i>Quercus</i>	oak		
<i>Ulmus</i>	elm		
<i>Abies</i>	fir		
<i>Acer</i>	maple		
<i>Salix</i>	willow		

## **Appendix 7: Pollen Concentrations For Pittsburg Basin and Catfish Pond**

Figures 7.5 and 7.6 show the relative pollen percentages for Pittsburg Basin and Catfish Pond. Here are graphs of the original pollen abundances for both sites. Data are courtesy of R. Teed.



